

Numerical modelling of thermally induced desiccation of geosynthetic clay liners observed in laboratory experiments

J. M. Southen¹ and R. K. Rowe^{2*}

¹Assistant Professor, Department of Civil Engineering, University of Western Ontario, London, Canada N6A 5B9, Telephone: +1 519 661 2111 Ext. 80113; Telefax: +1 519 661 3779
E-mail: jsouthen@eng.uwo.ca

²Professor and Canada Research Chair in Geotechnical and Geoenvironmental Engineering, GeoEngineering Centre at Queen's-RMC, Department of Civil Engineering, Queen's University, Kingston, ON, Canada K7L 3N6, Telephone: +1 613 533 3113, Telefax: +1 613 533 2128,
E-mail: kerry@civil.queensu.ca

*Corresponding author

Received 18 December 2008, revised 7 July 2011, accepted 8 July 2011

ABSTRACT: A fully coupled model is used to simulate the results of large-scale laboratory tests that investigated the non-isothermal behaviour of geosynthetic clay liners in landfill basal liner applications. Results of numerical simulations of the laboratory tests in terms of water content, capillary pressure, temperature and stress distributions are presented, and encouraging agreement between the numerical and experimental results is achieved. Under the conditions examined, a 25°C/m temperature gradient led to the development of tensile stresses within the GCL, increasing the resultant likelihood of cracking. A Poisson's ratio of 0.25 resulted in predicted horizontal tensile stresses supporting qualitative observation of desiccation cracking in the GCLs. One important implication of the work reported herein is that elevated temperatures need not occur for extended periods to create the risk of desiccation.

KEYWORDS: Geosynthetics, Geosynthetic clay liners, Desiccation, Temperature effects, Landfills, Liners, Moisture distribution

REFERENCE: Southen, J. M. & Rowe, R. K. (2011). Numerical modelling of thermally induced desiccation of geosynthetic clay liners observed in laboratory experiments. *Geosynthetics International*, 18, No. 5, 289–303. [<http://dx.doi.org/10.1680/gein.2011.18.5.289>]

1. INTRODUCTION

Landfill lining systems frequently include composite liners composed of a geomembrane and geosynthetic clay liner (GCL) (Koerner and Koerner 1999; Rowe *et al.* 2004). In these applications, the GCL serves to minimise advective transport of fluids through any holes in the geomembrane (Rowe 1998; Touze-Foltz *et al.* 2001, 2006; Touze-Foltz 2002; Giroud and Touze-Foltz 2003, 2005; Touze-Foltz and Giroud 2003, 2005; Rowe and Brachman 2004; Cartaud *et al.* 2005a, 2005b, 2005c; Iryo and Rowe 2005; Rowe 2005; Barroso *et al.* 2006; Bouazza and Vangpaisal 2006; Touze-Foltz and Barroso 2006; El-Zein and Rowe 2008; Bouazza *et al.* 2008, Saidi *et al.* 2008; Mendes *et al.* 2011b). However, the long-term effectiveness of the composite liner action will depend on

(a) the presence of holes and tensile strains (which can

give rise to future holes) in the geomembrane, especially in wrinkles in the geomembrane (Rowe 1998, 2005; Take *et al.* 2007; Thusyanthan *et al.* 2007; Brachman and Gudina 2008a, 2008b)

(b) the transmissivity of the geomembrane/GCL interface (Harpur *et al.* 1993; Rowe 1998; Rowe *et al.* 2004; Barroso *et al.* 2008, 2010; Mendes *et al.* 2011a)

(c) the hydraulic conductivity of the GCL (Rowe 1998; Rowe *et al.* 2004; Guyonnet *et al.* 2009; Rosin-Paumier *et al.* 2010a, 2010b; Paumier *et al.* 2010; Benson *et al.* 2010a, 2010b; Dickinson and Brachman 2010; Lange *et al.* 2010).

When hydrated, GCLs provide a very low-transmissivity geomembrane/GCL interface (Harpur *et al.* 1993; Rowe 2005; Barroso *et al.* 2008, 2010; Mendes *et al.* 2011a) and very low hydraulic conductivity (Rowe 2007). However,

the question arises as to whether this will be achieved in the long term, especially in light of the potential for high temperatures at the landfill base.

Municipal solid waste (MSW) incinerator bottom ash has also been found to cause liner temperatures of up to 46°C, owing to hydration of the ash (Klein *et al.* 2001). The degradation of organic matter within the waste mass is also an exothermic process that may result in significant heat generation. Under certain conditions, the heat generated by this process may raise the temperature within the waste mass to 70°C. The temperature on the liner in MSW may typically be 30–40°C (Rowe 2005; Koerner and Koerner 2006; Koerner *et al.* 2008). However, temperatures of 50–60°C have also been observed at the base of MSW landfills (Yoshida and Rowe 2003; Rowe 2005; Koerner *et al.* 2008). In contrast, the temperature of groundwater in underlying aquifers is typically 5–20°C.

When the top surface of a soil layer is heated, heat flows downwards, owing to the temperature gradient. Water vapour also moves towards areas of lower temperature, owing to variations in vapour density (Figure 1). As the migration of water vapour decreases the water content in the warmer area, capillary pressures develop, which cause liquid water to flow upwards towards the warmer area. However, the decrease in water content due to downward vapour flux results in a decrease in unsaturated hydraulic conductivity, which limits the rate at which liquid water can flow upwards to balance the downward flux of water vapour. This situation has the potential to result in significant decreases in water content at the upper surface, exacerbated by the presence of a practically impermeable geomembrane as the upper boundary. The large capillary pressures that may develop as a result have the potential to induce net tensile forces within the GCL, and thus a risk of desiccation cracking.

There are limited data regarding the desiccation potential of GCLs under thermal gradients. Numerical models have been developed by Döll (1996, 1997), Thomas and Missoum (1999) and Zhou and Rowe (2003) to describe the thermal desiccation behaviour of soils. Some experi-

mental investigations into the desiccation behaviour of GCLs in landfill cover applications (e.g. Sporer and Gartung 2002) have been performed, but little investigation has been done into the thermal desiccation behaviour of these materials in landfill basal liner applications. Southen and Rowe (2005a) have reported the results of experimental studies of GCL desiccation. The objective of this paper is to apply the Zhou and Rowe (2003) model for representing the desiccation behaviour of GCLs in landfill basal liner applications by comparing the predicted and observed behaviour for several laboratory experiments specifically designed to examine the potential for desiccation of GCLs in composite liner systems.

2. NUMERICAL MODEL

Methods for analysing the movement of moisture under non-isothermal conditions have traditionally been based on the model of Philip and de Vries (1957). This model uses temperature and water content as basic variables in the analysis of thermally driven moisture movement, subject to the assumptions of a rigid, homogeneous unsaturated medium. Milly (1982) extended the Philip and de Vries model, using temperature and capillary pressure (suction) as the basic variables. The use of capillary pressure rather than water content allows Milly's model to be used in the analysis of heterogeneous media. Döll (1996, 1997) implemented the Milly model in the SUMMIT model, and used it to investigate the desiccation potential in compacted clay liners used at the bottom of a landfill. Although Döll's development of the SUMMIT model represented a significant advance, its application is limited by the assumption of a rigid medium and the way in which vapour transport was modelled. A complete discussion of the applicability and limitations of the Döll model with respect to the analysis of GCL desiccation has been presented by Southen and Rowe (2005b) who concluded that, although the SUMMIT model is useful for making a general investigation into thermally induced moisture movement, a more complete model is necessary for extension of the investigation into cases involving composite liners containing GCLs.

Zhou and Rowe (2003) present a more complete model than that of Döll, which allows the analysis of deformable media. The reader is referred to Zhou and Rowe (2003) for full details of the model; only a brief summary and definition of key variables are given below. The stress state variables $(\sigma + p_a)$ and $(p_l - p_a)$ ($= p_c$) are used, where σ is total stress (tension positive), p_l is pore water pressure, p_a is air pressure and p_c is capillary pressure. The basic variables used are displacement (u), capillary pressure (p_c), air pressure (p_a) and temperature (T). The development of the model is as follows.

The equation for force equilibrium within the soil may be written as

$$(d\sigma_{ij})_{,j} + db_i = 0 \quad (1)$$

where σ_{ij} is the total stress in the ij direction (tension positive), and b_i is the body force in the i direction.

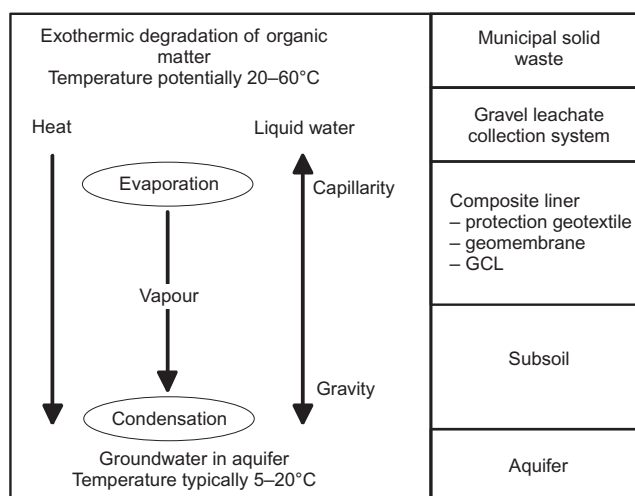


Figure 1. Mechanisms of thermally induced heat and mass flux beneath a landfill

The constitutive relationship is given by

$$d\sigma_{ij} = 2G \left(d\varepsilon_{ij} + \delta_{ij} \frac{\mu}{1-2\mu} d\varepsilon_{kk} \right) - KB_1 \delta_{ij} dp_c - \delta_{ij} dp_a - KB_2 \delta_{ij} dT \quad (2)$$

where ε_{ij} is the strain tensor, δ_{ij} is Kronecker's delta, G is the shear modulus, μ is Poisson's ratio, K is the bulk modulus of the soil ($= (\partial e / \partial \sigma) / (1 + e_0)$), B_1 is the compressibility of the soil due to changes in capillary pressure ($= (\partial e / \partial p_c) / (1 + e_0)$), and B_2 is the coefficient of thermal expansion ($= (\partial e / \partial T) / (1 + e_0)$).

The mass balance equation for water in a deformable unsaturated soil is given by

$$\frac{\partial \{ \rho_l (1 + e) \theta + \rho_v [e - (1 + e) \theta] \}}{(1 + e_0) \partial t} = -\nabla (q_l + q_v) \quad (3)$$

The mass balance equation for air in a deformable unsaturated soil is given by

$$\frac{\partial \{ \rho_{da} [e - (1 - H)(1 + e) \theta] \}}{(1 + e_0) \partial t} = -\nabla (q_{da}) \quad (4)$$

where t is time; e is the void ratio; e_0 is the initial void ratio; θ is the liquid volumetric water content; H is the coefficient of solubility of air into water (Henry's law); ρ_s , ρ_l , ρ_v and ρ_{da} are the densities of soil solids, liquid water, water vapour and dry air, respectively; q_l , q_v and q_{da} are the fluxes of liquid water, water vapour and dry air, respectively, and are given by

$$\begin{aligned} q_l &= -\rho_l \kappa_l \nabla (p_c + p_a + \rho_l g z) \\ q_v &= -D^* \nabla \rho_v - \rho_v k_a \nabla p_a \\ q_{da} &= -\rho_{da} [H \kappa_l \nabla (p_c + p_a + \rho_l g z) + k_a \nabla p_a] \end{aligned} \quad (5)$$

where κ_l is the mobility coefficient of liquid water associated with Darcy's law [$\kappa_l = K_l / (\rho_l g)$]; K_l is the hydraulic conductivity; g is gravitational acceleration; κ_a is the mobility coefficient of air; z is the vertical coordinate; and D^* is the effective molecular diffusivity of water vapour. κ_l and κ_a depend on the intrinsic permeability of the soil material, the degree of saturation, and the temperature.

The heat energy balance is given by

$$\frac{\partial \Phi}{(1 + e_0) \partial t} - (T + T_0) KB_2 \frac{\partial \varepsilon_v}{\partial t} = -\nabla q_T \quad (6)$$

where T_0 is the reference temperature ($^{\circ}\text{C}$) and ε_v is the volumetric strain.

The heat content Φ and total heat flux q_T due to conduction, convection and latent heat transfer can be expressed as:

$$\begin{aligned} \Phi &= \left\{ \begin{aligned} &\rho_s C_s + \rho_l C_l (1 + e) \theta + \rho_v C_v [e - (1 + e) \theta] \\ &+ \rho_{da} C_{da} [e - (1 - H)(1 + e) \theta] \end{aligned} \right\} T \\ &+ L_0 \rho_v [e - (1 + e) \theta] + \rho_l (1 + e) \theta W \end{aligned} \quad (7)$$

$$q_T = -\lambda' \nabla T + q_l C_l T + q_v C_v T + q_{da} C_{da} T + L_0 q_v \quad (8)$$

where C_s , C_l , C_v and C_{da} are the gravimetric specific heats of soil solids, liquid water, water vapour and dry air, respectively; L_0 is the latent heat of evaporation at the reference temperature; W is the differential heat of wetting associated with the exothermic process of wetting of the medium; and λ' is the Fourier thermal conductivity of the unsaturated medium.

Through manipulation of the balance equations and substitution of additional basic relationships, Zhou and Rowe (2003) arrive at the following balance equation systems:

$$\begin{aligned} (L_{11} + L_{21}) \frac{\partial \varepsilon_v}{\partial t} + (L_{12} + L_{22}) \frac{\partial p_c}{\partial t} \\ + (L_{13} + L_{23}) \frac{\partial p_a}{\partial t} + (L_{14} + L_{24}) \frac{\partial T}{\partial t} \\ = \nabla [(\rho_l \kappa_l + D_1^*) \nabla p_c] \\ + \nabla [(\rho_l \kappa_l + \rho_v \kappa_a + D_2^*) \nabla p_a] \\ + \nabla (D_3^* \nabla T) + \nabla [\rho_l \kappa_l \nabla (\rho_l g z)] \end{aligned} \quad (9)$$

$$\begin{aligned} L_{31} \frac{\partial \varepsilon_v}{\partial t} + L_{32} \frac{\partial p_c}{\partial t} + L_{33} \frac{\partial p_a}{\partial t} + L_{34} \frac{\partial T}{\partial t} \\ = \nabla (H \rho_{da} \kappa_l \nabla p_c) + \nabla [\rho_{da} (\kappa_a + H \kappa_l) \nabla p_a] \\ + \nabla [H \rho_{da} \kappa_l \nabla (\rho_l g z)] \end{aligned} \quad (10)$$

$$\begin{aligned} L_{41} \frac{\partial \varepsilon_v}{\partial t} + L_{42} \frac{\partial p_c}{\partial t} + L_{43} \frac{\partial p_a}{\partial t} + L_{44} \frac{\partial T}{\partial t} \\ = \nabla [D_{c2}^* \nabla p_c + D_{a2}^* \nabla p_a + D_{T2}^* \nabla T \\ + (C_l \rho_l + C_{da} \rho_{da} H) \kappa_l T \nabla (\rho_l g z)] \end{aligned} \quad (11)$$

where the full definitions of L_{ij} , D_1^* , D_2^* , D_3^* , D_{c2}^* , D_{a2}^* , and D_{T2}^* are given by Zhou and Rowe (2003).

Equations (1) combined with Equations (2) and (9)–(11) constitute a set of fully coupled governing equations describing the thermo-hydro-mechanical behaviour of unsaturated soils. These equations are non-linear, and must thus be solved numerically. Application of the finite element method to Equations (1), (9)–(11) in one-dimensional form results in (Zhou and Rowe 2003)

$$\begin{bmatrix} G_{11} & G_{12} & G_{13} & G_{14} \\ G_{21} & G_{22} & G_{23} & G_{24} \\ G_{31} & G_{32} & G_{33} & G_{34} \\ G_{41} & G_{42} & G_{43} & G_{44} \end{bmatrix} \begin{Bmatrix} \dot{u} \\ \dot{p}_c \\ \dot{p}_a \\ \dot{T} \end{Bmatrix} + \begin{bmatrix} 0 & 0 & 0 & 0 \\ 0 & K_{22} & K_{23} & K_{24} \\ 0 & K_{32} & K_{33} & 0 \\ 0 & K_{42} & K_{43} & K_{44} \end{bmatrix} \begin{Bmatrix} u \\ p_c \\ p_a \\ T \end{Bmatrix} = \begin{Bmatrix} \dot{F}_1 \\ F_2 \\ F_3 \\ F_4 \end{Bmatrix} \quad (12)$$

The coefficient matrices G and K depend on nodal variables, and are given by Zhou and Rowe (2003). Further details of the numerical method, including a full description of the mass-conservative finite element scheme used to evaluate the parameters in Equation (12), are given in Zhou and Rowe (2003). The model is verified by comparison with analytical and experimental data, as well as the numerical predictions of other models, in Zhou and Rowe (2003, 2005).

The model of Zhou and Rowe discussed above provides a general, fully coupled framework for analysis of the non-isothermal behaviour of unsaturated geosynthetic clay liners in landfill basal liner applications. The Zhou and Rowe model is one-dimensional, but this assumption is common, and is considered reasonable with respect to both temperature and deformations, provided there is an adequate protection layer to prevent local deformations due to gravel in the drainage layer, since the geomembrane and GCL are very thin compared with typical landfill dimensions. Even more relevant in the context of this paper is the fact that laboratory experiments to be modelled were designed to be one-dimensional, and there was no evidence of lateral movement of the GCL in the experiments prior to desiccation. One limitation of the model is that it does not explicitly simulate cracking, or the shrinkage that would occur once cracking is initiated. Strictly speaking, the model should not be run after the horizontal net stress drops below the point where cracking will occur. In particular, no great significance should be ascribed to tensile stresses once cracking has been initiated. However, the primary purpose of the model is to identify whether cracking is likely to occur; the limitation noted above does not affect the ability of the model to address this important practical question.

The model allows the simultaneous calculation of stress and deformation, thus facilitating study of the condition under which desiccation cracking may be initiated. In the following section the model is applied to the simulation of a series of large-scale laboratory experiments, the results of which were presented by Southen and Rowe (2005a). The constitutive relations and key material parameters are discussed in relation to the distribution of moisture, capillary pressure, temperature and stress observed in the large-scale tests.

3. MODELLING OF GCL DESICCATION

3.1. Laboratory testing

The results of a series of large-scale laboratory experiments designed to investigate the potential for thermally induced moisture movement within and beneath geosynthetic clay liners in landfill basal liner applications were presented by Southen and Rowe (2005a). The methodology employed in these experiments will be summarised briefly here. The goal of the experimental programme was to simulate reasonable worst-case landfill conditions. The tests utilised columns 1 m high and 30 cm in diameter. These columns were filled with a silty sand soil representative of a suitable subsoil for landfill construction. On top of this soil was placed a composite liner comprising a high-density polyethylene (HDPE) geomembrane and a GCL. The top and bottom of the column were sealed, and heat and pressure were applied to the upper surface; the lower surface was not heated. Insulation was provided around the exterior of the column to ensure that the thermal gradient developed through the system was one-dimensional.

Two subsoil materials (S1 and S2) and two GCL products (G1 and G2) were used in the large-scale experimental programme. The soils were silty sands with 12–19% silt content, optimum water content of 10–12%, and maximum dry density of 1.91–1.95 g/cm³. The first GCL, G1 (Bentofix NS), comprised a 4240 g/m² granular sodium bentonite core sandwiched between a 105 g/m² slit-film polypropylene woven carrier geotextile and a 200 g/m² polypropylene virgin staple fibre, needle-punched, nonwoven cover geotextile. The GCL was reinforced by needle-punching, and had thermally treated needle-punched fibres (thermal locking). The second GCL, G2 (Bentofix BFG 5000), differs from the first in that the core contains 5000 g/m² of powdered sodium bentonite, and the cover nonwoven geotextile is impregnated with 800 g/m² of bentonite. The carrier geotextile is a 200 g/m² polypropylene slit-film woven, while the cover geotextile is a 300 g/m² polypropylene, needle-punched, nonwoven.

A full description of the experimental procedure and results may be found in Southen and Rowe (2005a). Eight experiments were conducted as part of the laboratory programme. To present concisely the key issues associated with utilising the model of Zhou and Rowe (2003), the results from two large-scale experiments using each of the GCL and subsoil materials are presented in this paper. Table 1 gives pertinent data regarding experimental details. Measurements taken at the end of the experiments indicate that, for the conditions analysed, the potential for desiccation of a GCL in a composite liner subjected to a thermal gradient does exist. The tests gave final GCL volumetric water contents between 0.09 and 0.23. Observations of the GCLs following these tests indicated that significant desiccation cracking had occurred. Additional tests conducted with higher initial subsoil water contents discussed by Southen and Rowe (2005a) did not show signs of desiccation within the GCL. The Zhou and Rowe (2003) model was used to simulate these experiments as

Table 1. Laboratory test details

Test	Pre-heat duration (days)	Test duration (days)	Initial subsoil volumetric water content	Initial subsoil dry density (g/cm ³)	Initial GCL volumetric water content	Applied pressure (kPa)	Applied temperature gradient (°C/m)	Final GCL volumetric water content	Final subsoil volumetric water content
G1-S1-L5	50	232	0.07	1.75	0.71	50	27	0.09	0.004–0.16
G2-S2-L3	49	233	0.11	1.79	0.46	70	24.8	0.23	0.005–0.29

well (Southen 2005). The model indicated that no cracking was expected in these cases, and so the results are not presented here, in the interests of demonstrating the capability of the model more succinctly in cases where desiccation does occur.

3.2. Constitutive relations and material parameters

In order to use the model of Zhou and Rowe (2003), it is necessary to obtain various parameters that describe the physical relationships within the deformable media. Parameters are required for equations describing the state surface, the soil water characteristic curve, the thermal coefficient of volume change, the unsaturated hydraulic conductivity function, and the thermal conductivity. Often, such parameters are difficult to obtain experimentally, and there is a paucity of data reported in the literature, especially with respect to geosynthetic clay liners. In this section, the constitutive relations are presented, along with the parameters used to describe the behaviour of the GCL and silty sand subsoil. Justification for the chosen parameters is made with respect to experimental data where available. Table 2 summarises the parameters used to model the laboratory experiments.

3.2.1. State surface

The following state surface has been shown to give a reasonable representation of the behaviour of deformable, unsaturated soils (Lloret and Alonso 1985; Thomas *et al.* 1996):

$$e = a + b \ln(-\sigma) + c \ln(-p_c) + d \ln(-\sigma) \ln(-p_c) + (1 + e_0) \alpha_T \Delta T \quad (13)$$

where e is the void ratio; e_0 is the initial void ratio; σ is

the net mean stress; p_c is the capillary pressure; ΔT is the temperature increase; α_T is the thermal coefficient of volume change (Section 3.2.5); and a , b , c and d are model parameters. The parameters a , b and d were chosen based on published swelling data for the GCLs, and on consolidation testing for the silty sand. Figure 2 plots the state surfaces in the e – σ plane. The experimental data for the GCLs were taken from the work of Lake and Rowe (2000) who conducted swell tests on GCL specimens nearly identical to those used in the large-scale tests. In the figure, CSST refers to constant stress swell tests, and CVST refers to constant-volume swell tests. The inset to Figure 2 gives the deformation behaviour of the S1 subsoil material measured in a standard consolidation test (ASTM D 2435-04). While the log-linear relationship appears to be a good fit to the GCL data over the range of capillary pressures studied, it is a simplification for the bi-linear relationship evident in the silty sand results. An effort was made to give the best fit to data in the 50–1000 kPa stress range, as this is typical of the overburden pressures likely to be encountered in landfill basal liner applications. The two silty sand subsoils did not show significant variation in compressibility, so the parameters adopted for S2 were the same as for S1.

The effect of capillary pressure on void ratio (as included in Equation (13) by parameters c and d) may be inferred from observations made during the soil water characteristic curve (water retention curve) testing reported by Southen and Rowe (2007). For tests conducted on the silty sand soils S1 and S2, no evidence of volume change was noted over the range of capillary pressures examined: thus the silty sand was assumed to have very low compressibility with respect to changes in capillary pressure. The influence of suction on the void ratio of the

Table 2. Model parameters

	a	b	c	D	a'	b'	c'	d'
S1	0.660	–0.013	–0.0001	1.0×10^{-5}	1.0	0.986	0	3.0×10^{-5}
S2	0.640	–0.013	–0.0001	1.0×10^{-5}	1.0	0.985	0	4.2×10^{-5}
G1	8.90	–0.590	–0.310	0.025	1.0	0.93	-1.55×10^{-6}	1.7×10^{-7}
G2	14.0	–1.0	–0.385	0.025	1.0	0.90	-2.5×10^{-6}	1.8×10^{-7}
	A	S_{ru}	α_k	α_T	λ_{dry}	λ_{sat}	μ	
S1	1.0×10^{-6}	0.02	–2.5	Varies	0.50	3.50	Varies	
S2	5.0×10^{-7}	0.0	–2.5	Varies	0.50	3.50	Varies	
G1	3.0×10^{-11}	–0.40	0.001	Varies	0.10	0.80	Varies	
G2	3.0×10^{-11}	–1.0	0.001	Varies	0.10	0.80	Varies	

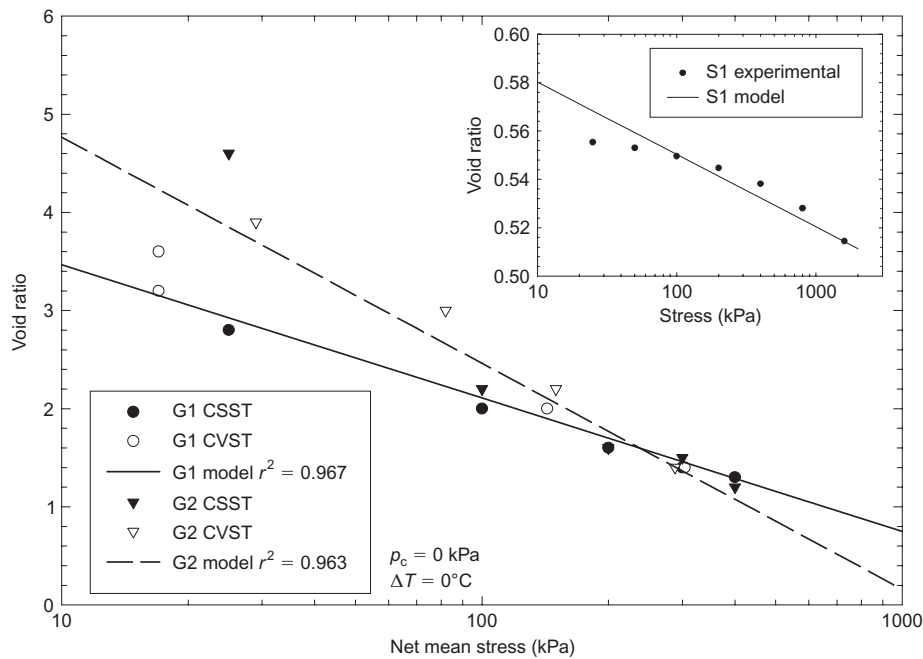


Figure 2. State surface representation for GCLs G1 and G2 and silty sand S1

GCLs was inferred based on observations of the change in void ratio during the soil water characteristic curve testing reported by Southen and Rowe (2007). The model assumes a log-linear relationship between capillary pressure and void ratio, with a slope determined by the best fit to the experimental data using the c and d parameters of Equation (13). Similar to the $e-\sigma$ relationship, this representation may be seen as a simplification of the bi-linear or tri-linear $e-p_c$ curves suggested by Fleureau *et al.* (1993, 2002), which are analogous to the consolidation behaviour of an overconsolidated clay. Although Equation (13) is not an exact representation of the state surface of compressible soils, it may be seen as a useful empirical relationship that facilitates the numerical modelling procedure. Further refinement of the model of Zhou and Rowe (2003) may be necessary to better capture the behaviour of highly compressible materials. The thermal coefficient of volume change (α_T) is discussed further in Section 3.2.5.

3.2.2. Soil water characteristic curve (water retention curve)

The soil water characteristic curve may be defined using the equation given by Lloret and Alonso (1985),

$$\theta = \frac{e}{1 + e_0} [a' - (b' - c'\sigma) \tanh(-d' p_c)] \quad (14)$$

where θ is the liquid volumetric water content, and a' , b' , c' and d' are model parameters. Soil water characteristic curves were obtained for the GCLs using the axis-translation technique with a pressure membrane extractor, as discussed by Southen and Rowe (2007). Curves were obtained under applied loads of 0.5, 3 and 100 kPa to assess the effect of stress on Equation (14). Figure 3 shows the experimental and model soil water characteristic curves in terms of degree of saturation (S_r), where

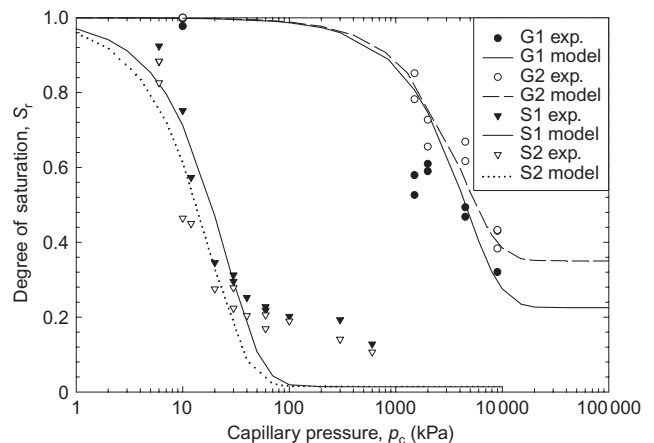


Figure 3. Soil water characteristic curves for GCL G1 and G2 (under 100 kPa load) and silty sand S1 and S2

$S_r = \theta(1 + e)/e$, for tests on GCLs G1 and G2 conducted under an applied load of 100 kPa. Curves for the two silty sand materials were obtained using a pressure plate extractor under zero applied stress conditions, as discussed by Southen and Rowe (2007). The model of Lloret and Alonso is limited in its ability to represent accurately the soil water characteristics of the materials used in the current study (Figure 3). The fit to the silty sand data is especially poor at high capillary pressures, and the curve for the GCL places an artificial limit on the minimum degree of saturation, which theoretically approaches zero at capillary pressures approaching 10^6 kPa (Fredlund and Rahardjo 1993). Equation (14) was incorporated into the Zhou and Rowe model for reasons of numerical stability, but consideration should be given to the adoption of alternative representations of the soil water characteristic curve (e.g. Fredlund and Xing 1994) in future revisions of the model, if it can be extended to account for the effect

of applied stress on a GCL, to improve the accuracy of the results. Although there has been recent progress in the development of techniques for establishing the advances in the soil water characteristic curve for GCLs (Abuel-Naga and Bouazza 2010; Beddoe *et al.* 2010, 2011), there is still a paucity of data regarding the effect of stress on the soil water characteristic curve for GCLs that is needed to improve the constitutive relationship in the Zhou and Rowe (2003) model; this is an important topic for future research.

The effect of temperature on the soil water characteristic curve is accounted for by using a temperature-corrected capillary pressure term p_{cc} that is assumed to be a function of capillary pressure and temperature (Milly 1984), given by

$$p_{cc} = p_c \exp(-C_{pc} T) \quad (15)$$

where C_{pc} is the temperature coefficient of water retention ($^{\circ}\text{C}^{-1}$). The value of C_{pc} is taken as $0.0068^{\circ}\text{C}^{-1}$, based on Scanlon and Milly (1994).

3.2.3. Unsaturated hydraulic conductivity function

The unsaturated hydraulic conductivity function for an unsaturated soil may be taken as (Alonso *et al.* 1988)

$$K_l = \kappa_l \rho_l g = A \left[\frac{S_r - S_{ru}}{1 - S_{ru}} \right]^3 10^{\alpha_k e} \quad (16)$$

where K_l is the unsaturated hydraulic conductivity; S_r is the degree of saturation; and A , S_{ru} and α_k are model constants. The unsaturated hydraulic conductivity function is very difficult and time-consuming to obtain. To obtain model parameters that give a reasonable approximation, Equation (16) was fitted to curves obtained using the van Genuchten–Mualem equation (van Genuchten 1980). The most appropriate description of the unsaturated hydraulic conductivity function for the materials under consideration was chosen based on the results of numerical modelling using the Döll model presented by Southen and Rowe (2005b). Figure 4 gives the curves obtained in this fashion for the two GCL products and the two silty sands. An

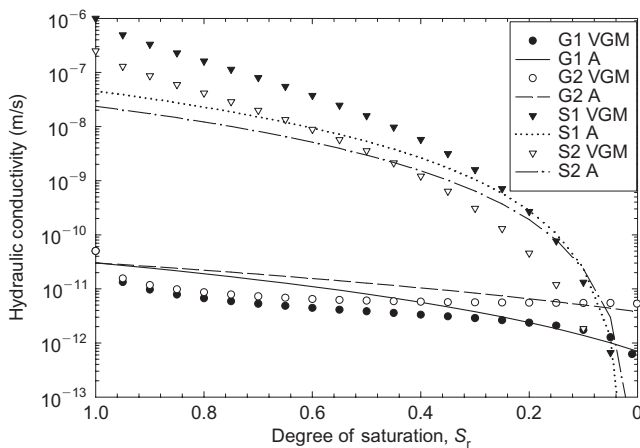


Figure 4. Unsaturated hydraulic conductivity function for GCLs G1 and G2 and silty sands S1 and S2

effort was made to fit the curves most accurately where the degree of saturation is lower, since this is the region of primary concern when considering desiccation behaviour. The effect of temperature on the unsaturated hydraulic conductivity function is accounted for by modifying the mobility coefficient of water to consider capillary pressure temperature correction and the change in water viscosity in a similar manner to that discussed for the soil water characteristic curve in Section 3.2.2.

3.2.4. Thermal conductivity

The thermal conductivity of unsaturated soil may be approximated by

$$\lambda' = \lambda_{dry}(1 - S_r) + \lambda_{sat}S_r \quad (17)$$

where λ_{dry} and λ_{sat} are the coefficients of thermal conductivity of the soil when completely dry and fully saturated, respectively. To estimate λ_{dry} and λ_{sat} , the method of de Vries (1975) and Milly (1984) was used. This method involves a weighted average of the thermal conductivities of the constituent phases, namely liquid water, air and soil solids. The thermal conductivity of air was taken as $0.025 \text{ W}/(\text{m}^{\circ}\text{C})$, and that of water was taken as $0.57 \text{ W}/(\text{m}^{\circ}\text{C})$. For the GCLs, the thermal conductivity of the soil solids was taken as $2.0 \text{ W}/(\text{m}^{\circ}\text{C})$, and that of the geotextile component was $0.12 \text{ W}/(\text{m}^{\circ}\text{C})$. The thermal conductivity of the soil solids within the silty sand was taken to be $7.0 \text{ W}/(\text{m}^{\circ}\text{C})$, which corresponds to solid grains made up of $\sim 70\%$ quartz. The thermal conductivities of the various constituents are taken from de Vries (1975), Milly (1984), Neiß (1982) and Farouki (1986).

3.2.5. Thermal coefficient of volume change

The thermal coefficient of volume change (α_T) used in Equation (13) can be expressed as (Thomas *et al.* 1996):

$$\alpha_T = \alpha_0 + \alpha_2 T + (\alpha_1 + \alpha_3 T) \ln \left(\frac{\sigma}{\sigma_0} \right) \quad (18)$$

where σ_0 is the reference stress, and α_0 , α_1 , α_2 , and α_3 are model parameters. Limited data exist regarding the change in volume of unsaturated soils with regard to temperature changes. Delage *et al.* (2000) present a discussion on thermal effects for saturated clays, suggesting an inverse relationship between void ratio and temperature due to changes in the thickness of bound water. Devillers *et al.* (1996) and Saix *et al.* (2000) investigate the influence of temperature on void ratio under oedometric conditions for unsaturated clayey silty sand. They conclude that thermal consolidation occurs in two stages, analogous to the mechanical behaviour of overconsolidated clay: that is, $\Delta e = -C_{T1} \log(T_L/T_i) + C_{T2} \log(T_f/T_L)$. Up to a limiting temperature (T_L) of approximately 40°C , changes in temperature had a relatively small effect on void ratio, with a thermal compression index (C_{T1}) of approximately 0.02. Above this threshold, increased temperature led to more significant reductions in void ratio, with a thermal compression index (C_{T2}) of between 0.05 and 0.08. No reported investigations into the behaviour of unsaturated soils with low clay content (such as the silty sand used in the present study) were found. Because of

this uncertainty, a range of parameters was used in the modelling, as discussed in Section 3.3.4.

3.2.6. Poisson's ratio

An estimate of the Poisson's ratio of the unsaturated soil is required for the Zhou and Rowe model to calculate shear and elastic moduli based on the bulk modulus, as well as to calculate horizontal stresses. Assuming elastic isotropy for the soil, the Poisson's ratio μ is related to the bulk modulus K and shear modulus G of the soil by

$$\mu = \frac{3K - 2G}{6K + 2G} \quad (19)$$

In the Zhou and Rowe model, the bulk modulus is calculated based on the parameters b and d used in Equation (13). The value of K is then used to calculate the shear modulus using Equation (19) for a specified Poisson's ratio. Limited data exist regarding the Poisson's ratio for unsaturated soils of the type used in the current study. A survey of reported values for surface soils determined from seismic wave velocities reported by Salem (2000) indicates a range of Poisson's ratio of between 0 and 0.45, with an average value of 0.35. The value of Poisson's ratio was thus varied in the modelling to obtain the best fit with experimental results, as discussed further in Section 3.3.4.

3.2.7. Diffusion coefficients

The coefficients governing the diffusion of water vapour due to gradients of capillary pressure, temperature and air pressure are calculated in the same manner as is used in the Döll model by Southen and Rowe (2005b). The general equation for the effective diffusion coefficient D^* is given by

$$D^* = f(\theta)\tau D_{\text{atm}}(T, p_a) \quad (20)$$

where D^* represents the effective diffusion coefficient in question, $f(\theta)$ is the effective porosity, τ is tortuosity, and D_{atm} is the vapour diffusion coefficient in free air. The parameters F_v and $\xi(\theta)$ are used when calculating the vapour diffusion coefficient with respect to temperature gradients, where $\xi(\theta)$ is the temperature gradient ratio (accounting for the difference between the bulk temperature gradient and the higher temperature gradient in air-filled pores), and F_v is the vapour diffusion enhancement coefficient:

$$D_3^* = F_v \xi(\theta) f(\theta) \tau D_{\text{atm}} \left. \frac{\partial \rho_v}{\partial T} \right|_{p_c} \quad (21)$$

In the Zhou and Rowe model, F_v is set to unity (i.e. enhanced thermal vapour diffusion is not considered), and the calculation of $\xi(\theta)$ follows the procedure given by Döll (1996). More detail regarding these parameters may be found in Southen and Rowe (2005b) and Zhou and Rowe (2003).

Based on the above points, parameters were chosen to represent the behaviour of the two GCL products, G1 and G2, and the two silty sand subsoil materials, S1 and S2, as given in Table 2.

3.3. Results

The two large-scale laboratory tests, G1-S1-L5 and G2-S2-L3, were modelled using the parameters given in Table 2. The problem was analysed using a finite element mesh containing 160 one-dimensional, two-node elements. The GCL was modelled as a layer 0.008 m thick using 40 elements, and the subsoil was divided into layers 0.025, 0.075 and 0.90 m thick using 50, 25 and 45 elements, respectively. All elements are uniformly distributed within each layer. Simulations were run using a total of 80, 160 and 320 elements to check mesh refinement. It was found that 80 elements were not sufficient to achieve accurate results, but adding elements beyond 160 did not significantly change the results. For each test the top boundary conditions were zero moisture flux and prescribed temperature and stress increases, based on the test details. The bottom boundary conditions were prescribed temperature, zero moisture flux, and zero displacement. Given the two distinct stages of the test (i.e. the isothermal pre-heat and non-isothermal heating stages), the program implementing the Zhou and Rowe (2003) model was first run with the boundary conditions for the isothermal stage of the laboratory tests, and the results were used as initial conditions for a second run with boundary conditions for the non-isothermal stage.

3.3.1. Water content and capillary pressure

Figure 5 shows the variation in volumetric water content with depth at placement, at the beginning of heating and at termination for tests G1-S1-L5 and G2-S2-L3. As indicated in Table 1, the subsoil in test G1-S1-L5 was placed at an initial volumetric water content of 0.073, and the subsoil in test G2-S2-L3 was placed at an initial volumetric water content of 0.113. The GCL in test G1-S1-L5 was placed at an initial volumetric water content of 0.713, whereas for test G2-S2-L3 the GCL was placed at an initial volumetric water content of 0.458. Figure 5 shows that during the isothermal pre-heating stage of these tests, the GCL took up water from the underlying subsoil to approach saturated levels. Moisture redistribution took place within the subsoil under gravitational forces, such that the volumetric water content decreased by 0.007–0.02 in the upper portion of the subsoil and increased by 0.005–0.015 at the base.

Following 232–233 days of heating there were significant reductions in GCL water content. The GCL in test G1-S1-L5 decreased in volumetric water content to 0.095, and in test G2-S2-L3 the final GCL volumetric water content is 0.176. Within the subsoil, the volumetric water content at the GCL interface reduced to residual values of 0.0048 for test G1S1 and 0.0050 for test G2-S2-L3. The volumetric water contents predicted by the numerical model (Figure 5) fit the general trends observed in the experimental data, and agreement is especially good within the GCL and in the upper 5 cm of the subsoil. Deviations from experimentally observed volumetric water contents within the subsoil are probably due to the generally poor fit obtained when fitting Equation (14) to the experimental soil water characteristic curve data, especially for the silty sand.

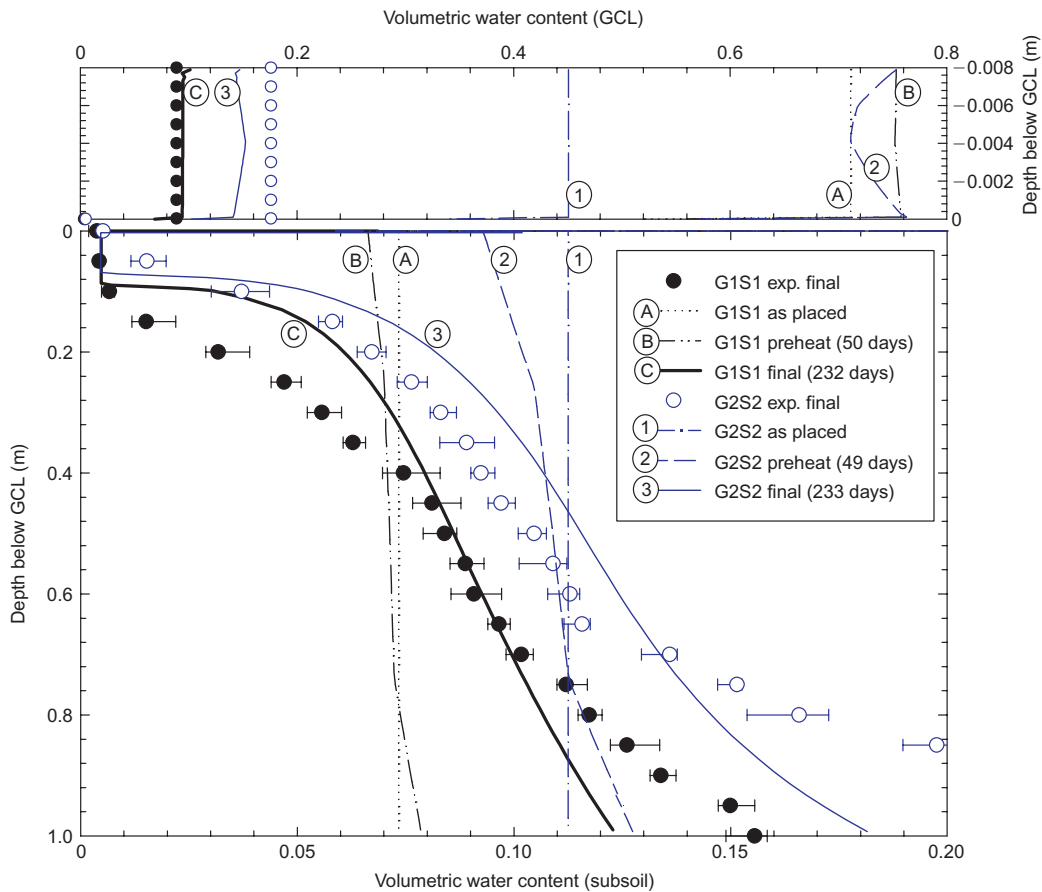


Figure 5. Calculated and observed volumetric water content profiles for G1-S1-L5 and G2-S2-L3

The distribution of water content is closely related to the variation of capillary pressure within the soil. Figure 6 shows the predicted capillary pressure profiles for tests G1-S1-L5 and G2-S2-L3. Large changes in capillary pressure occurred with depth to approximately 0.1 m below the GCL, at which point the variation became more modest with depth. For G1-S1-L5 (Figure 6), the capillary pressure changed rapidly from approximately 50 kPa at a depth of 0.1 m to approximately 60 000 kPa at the GCL interface. With reference to Figure 3, it is within the range of capillary pressure from 10 to 100 kPa that the silty sand

undergoes an extreme change in water content. As vapour flow transports moisture downwards, the reduction in water content in this range led to a decrease in unsaturated hydraulic conductivity by several orders of magnitude (Figure 4), which limited the upward transport of liquid water needed to offset the downward vapour flow. This resulted in further reductions in water content and hydraulic conductivity, exacerbating the degree of desiccation.

Figure 7 shows the predicted temporal variation of (a) water content and (b) capillary pressure at different depths for test G2-S2-L3. Desaturation occurred rapidly within the upper subsoil, and the residual water content was reached within 40 days after the start of heating (although the capillary pressure continued to increase after this time). The GCL also experienced a relatively rapid reduction in water content. The decline in volumetric water content from 0.71 initially to 0.61 after 1 day may be attributed to a reduction in void ratio caused by the applied overburden stress, since no corresponding increase in capillary pressure was noted during this period. Changes in volumetric water content and capillary pressure within the GCL became less pronounced after approximately 200 days. This suggests that elevated temperatures need not occur for extended periods to create the risk of desiccation.

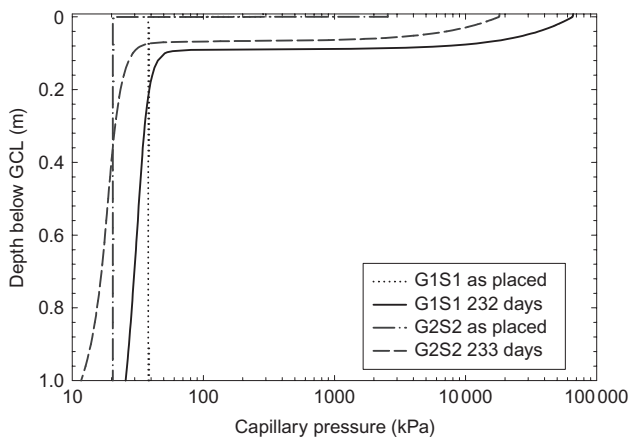


Figure 6. Calculated capillary pressure profiles for G1-S1-L5 and G2-S2-L3

3.3.2. Temperature

The experimental observations and the calculated temperatures are shown in Figure 8. The temperature gradient

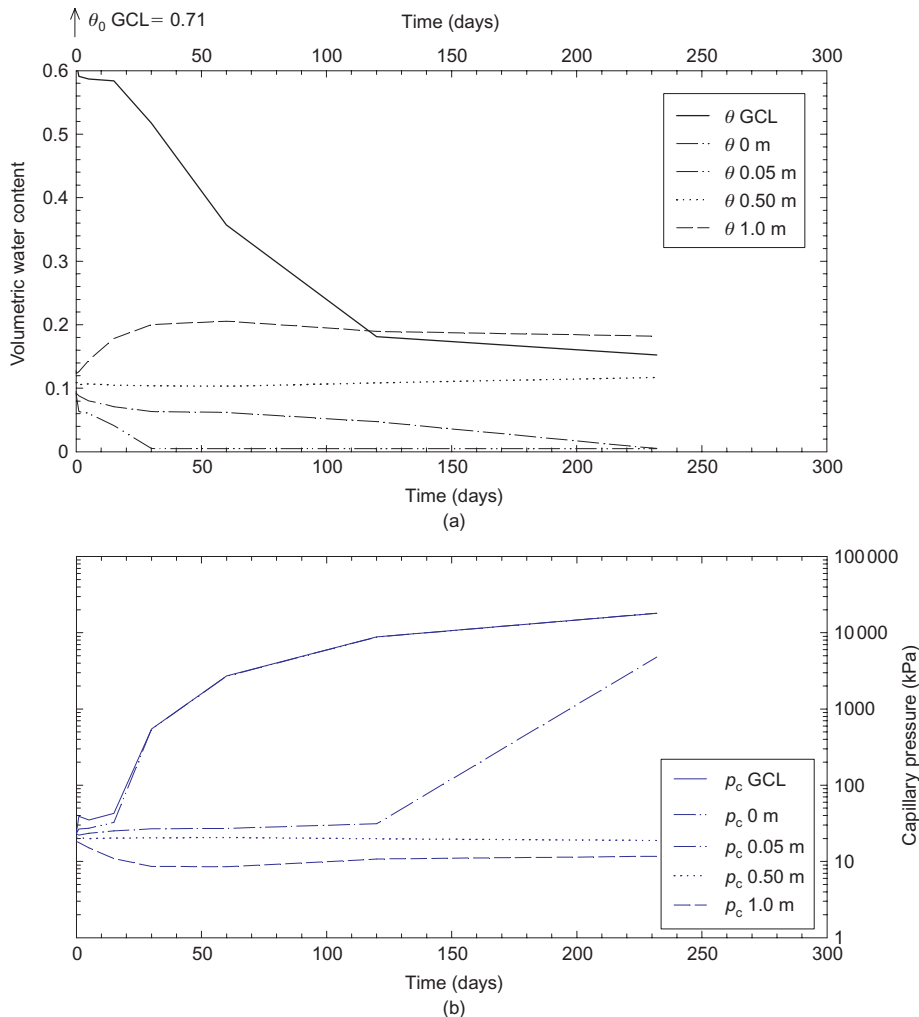


Figure 7. Calculated temporal variation of (a) volumetric water content and (b) capillary pressure at various depths for G2-S2-L3

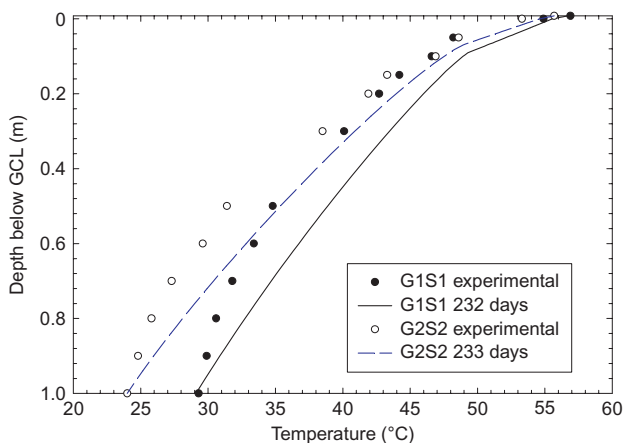


Figure 8. Calculated and observed temperature profiles for G1-S1-L5 and G2-S2-L3

decreased with depth, due primarily to the direct relationship between the thermal conductivity of the subsoil and its water content. The numerical model performed reasonably well, although the temperature gradient in the upper portion was underpredicted.

3.3.3. Deformation

One of the advantages of the Zhou and Rowe (2003) model is the assumption of a deformable medium. As indicated in Figure 2, GCLs are extremely compressible, and thus it is necessary to account for deformation. Table 3 gives the initial and final GCL void ratios observed for tests G1-S1-L5 and G2-S2-L3. Significant reductions in void ratio were observed. Also presented in Table 3 are the final void ratios predicted by the model for each test. The predicted void ratios are nearly identical to those observed. A model that does not take such deformation into account is not suitable for the prediction of GCL desiccation.

3.3.4. Stress

The model of Zhou and Rowe allows the simultaneous calculation of stress and deformation, which facilitates the

Table 3. Variation in GCL void ratio

Test	e_0	e_f	$e_{f\text{predicted}}$
G1S1	2.62	1.76	1.78
G2S2	2.88	0.99	0.98

evaluation of desiccation potential. The calculated variation of net total horizontal stress ($\sigma_H + p_a$) with depth is shown in Figure 9 for tests G1-S1-L5 and G2-S2-L3 with $\mu = 0.25$ for both materials, $\alpha_{TGCL} = -0.0002$ and $\alpha_{TSS} = 0$. The Poisson's ratio and thermal coefficient of volume change used are discussed in detail below. Test G1-S1-L5 was conducted with an applied overburden stress of 50 kPa, whereas a 70 kPa overburden stress was applied in test G2-S2-L3. A concentration of stress within the GCL was predicted for test G2-S2-L3, owing to swelling (expansion) of the GCL as it hydrates. Capillary pressure had relatively little effect on the predicted horizontal stress within the subsoil, since the compressibility of the silty sand with respect to changes in capillary pressure was very low (see Table 2, parameters c and d). In contrast, the GCLs were found to have significant compressibility with respect to changes in capillary pressure. As a result, the high capillary pressures noted in Section 3.2.1 give rise to the development of tensile horizontal stresses within the GCLs. Air pressure (p_a) was atmospheric at the beginning and end of the tests, such that the net total stresses were equal to the total stresses at these times. Some transient variation in air pressure was noted, although the effects were minor.

As discussed in Sections 3.2.5 and 3.2.6, parameters for the thermal coefficient of volume change (α_T) and Poisson's ratio (μ) are not well defined. To examine the effect of these parameters, they were varied within a range of reasonable values. Poisson's ratios of 0.25, 0.30 and 0.35 were chosen for both the silty sand and the GCL. The value of α_T was chosen based on a linear fit of the

logarithmic coefficients given by Devillers *et al.* (1996). For the silty sand subsoil, values of 0.00025, 0 and -0.0002 were used, and the GCL had values of 0 and -0.0002 . The chosen value of α_T had a significant effect on the predicted horizontal stresses within the subsoil. For $\alpha_{TSS} = 0.00025$ thermal expansion of the subsoil under elevated temperatures resulted in larger compressive stresses at the GCL interface, decreasing gradually with depth. For $\alpha_{TSS} = -0.0002$ the reverse was true, with more tensile stress induced at the upper boundary. The results given in Figure 9 are those with $\alpha_{TSS} = 0$. Changes in α_{TSS} had relatively little effect on predicted horizontal stresses within the GCL, and practically no effect on predicted suctions, water contents or temperatures was noted within either material.

Figure 10 shows the predicted net total horizontal stress within the GCL for a range of Poisson's ratio and α_T . As may be expected, a decrease in the Poisson's ratio resulted in less compressive horizontal stress within the GCL. Changes in the thermal coefficient of volume change of the subsoil had practically no effect on the predicted stresses within the GCL (compare B and C), and changes in the thermal coefficient of volume change of the GCL had only a modest effect (compare A and B/C). It is generally assumed that cracking occurs when the net total horizontal stress within the soil becomes more tensile than the tensile strength of the soil (Morris *et al.* 1992). No data could be found in the literature regarding the tensile strength of the mineral component of GCLs, but a conservative approach would be to assume zero tensile strength (i.e. that cracking is initiated when the horizontal

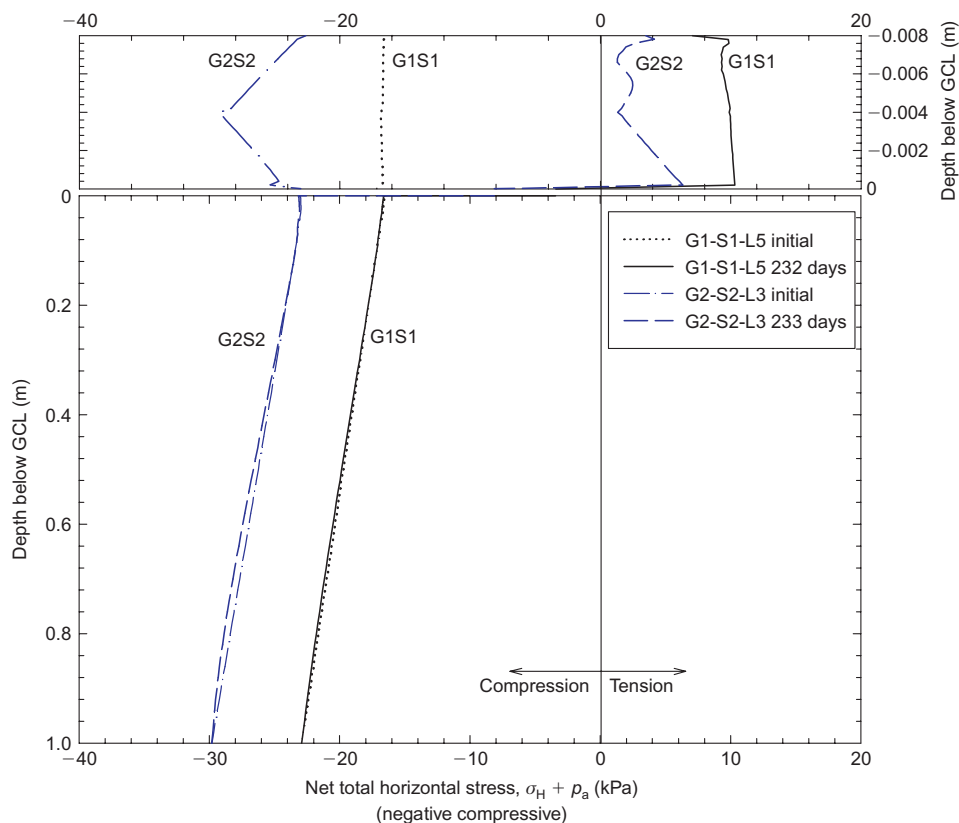


Figure 9. Net total horizontal stress profiles for G1-S1-L5 and G2-S2-L3

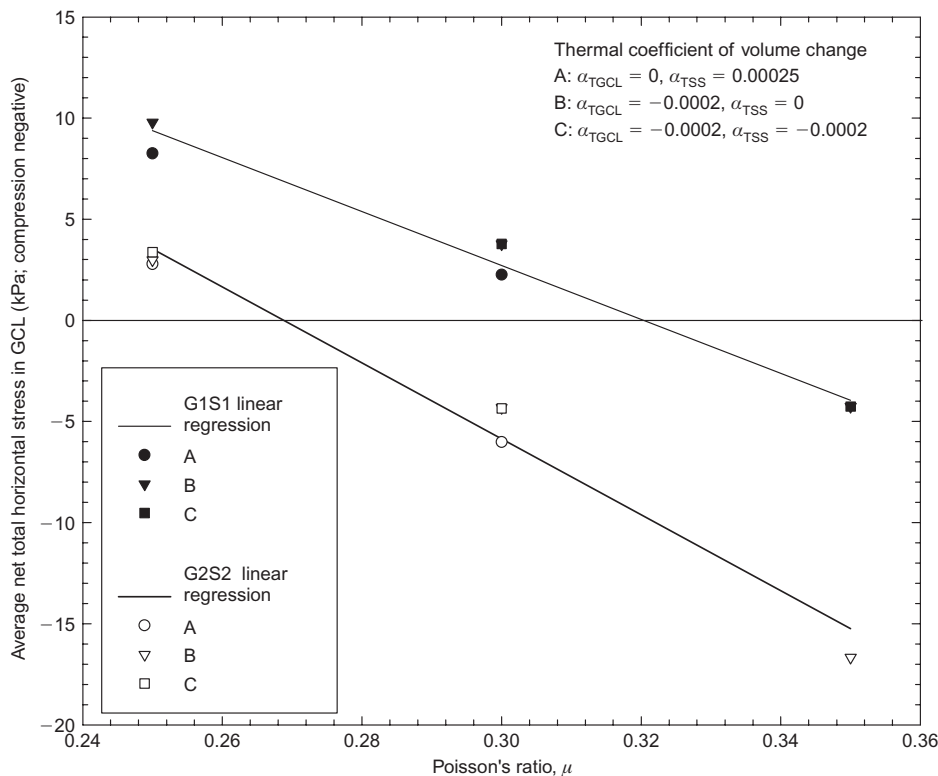


Figure 10. Influence of Poisson's ratio (same for both materials) and thermal coefficient of volume change on predicted net total horizontal stress ($\sigma_H + p_a$) within GCL for G1-S1-L5 and G2-S2-L

stress within the GCL becomes tensile). From Figure 10 it can thus be said that for cracking to occur under the conditions analysed, the Poisson's ratio of GCL G1 must be less than ~ 0.32 , and that of G2 must be less than ~ 0.27 . Since cracking was observed throughout the thickness of the GCL for both tests G1-S1-L5 and G2-S2-L3, a Poisson's ratio of 0.25 was taken to be appropriate. This value is in agreement with some limited data for sensitive clays reported in the literature (e.g. Ghahremannejad 2003).

4. CONCLUSION

The fully coupled model of Zhou and Rowe (2003) was used to simulate the results of large-scale laboratory tests that investigated the non-isothermal behaviour of geosynthetic clay liners in landfill basal liner applications. A set of constitutive equations and material parameters were presented that define the thermal, mechanical and hydraulic behaviour of two silty sand and two GCL materials. These relationships were used to calibrate the numerical model. Results of numerical simulations of the laboratory tests in terms of water content, capillary pressure, temperature and stress distributions were presented. In addition, the deformation of the GCLs was discussed. Encouraging agreement between the numerical and experimental results was achieved.

Under the conditions examined, a $25^\circ\text{C}/\text{m}$ temperature gradient led to the development of capillary pressures in excess of 10 MPa within the GCL and upper portion of

the subsoil. This capillary pressure resulted in the development of tensile stresses within the GCL, increasing the resultant likelihood of cracking. Based on a parametric investigation, the Poisson's ratio was found to be a governing factor in horizontal stress development, with the thermal coefficient of volume change playing a secondary role. A Poisson's ratio of 0.25 resulted in predicted horizontal tensile stresses supporting qualitative observation of desiccation cracking in the GCLs.

One important implication of the work reported herein is that elevated temperatures need not occur for extended periods to create the risk of desiccation.

The results of the numerical analyses suggest that the Zhou and Rowe (2003) model is suitable for investigations of the desiccation behaviour of deformable unsaturated soils. A set of parameters has been presented that allows simulation of thermally induced moisture movement within and beneath GCLs as part of a landfill composite lining system.

ACKNOWLEDGEMENTS

The research presented in this paper was funded by Terrafix Geosynthetics Inc., the Centre for Research in Earth and Space Technology (CRESTech), and the Natural Sciences and Engineering Research Council of Canada (NSERC). In addition, the value of discussions with K. von Maubeuge of Naue Fasertechnik and B. Herlin of Terrafix Geosynthetics Inc. is gratefully acknowledged.

NOTATIONS

Basic SI units are given in parentheses.

A	parameter for unsaturated hydraulic conductivity function (m/s)	T_L	limiting temperature in thermal consolidation equation ($^{\circ}\text{C}$)
a, b, c, d	parameters for state surface of void ratio (dimensionless)	t	time (s)
a', b', c', d'	parameters for soil water characteristic curve (dimensionless)	u	displacement (m)
B_1	compressibility of soil due to changes in capillary pressure (m^2/N)	u_i	displacement in the i th direction (m)
B_2	coefficient of thermal expansion ($^{\circ}\text{C}^{-1}$)	W	differential heat of wetting (J/kg)
b_i	body force in the i th direction (N/m^3)	z	vertical coordinate (m)
C_{da}	gravimetric specific heat of dry air ($\text{J}/(\text{kg } ^{\circ}\text{C})$)	α_T	thermal coefficient of volume change ($^{\circ}\text{C}^{-1}$)
C_l	gravimetric specific heat of liquid water ($\text{J}/(\text{kg } ^{\circ}\text{C})$)	α_k	parameter for unsaturated hydraulic conductivity function (dimensionless)
C_{pc}	temperature coefficient of water retention ($^{\circ}\text{C}^{-1}$)	α_0, α_1	parameters for thermal coefficient of volume change ($^{\circ}\text{C}^{-1}$)
C_s	gravimetric specific heat of soil solids ($\text{J}/(\text{kg } ^{\circ}\text{C})$)	α_2, α_3	parameters for thermal coefficient of volume change (dimensionless)
C_{T1}	primary thermal consolidation index (for temperatures below T_l) (dimensionless)	δ_{ij}	Kronecker's delta (dimensionless)
C_{T2}	secondary thermal consolidation index (for temperatures above T_l) (dimensionless)	ε_{ij}	strain tensor (dimensionless)
C_v	gravimetric specific heat of water vapour ($\text{J}/(\text{kg } ^{\circ}\text{C})$)	ε_v	volumetric strain (dimensionless)
D_{atm}	vapour diffusion coefficient in free air (m^2/s)	θ	liquid volumetric water content (dimensionless)
D^*	effective molecular diffusivity of water vapour (m^2/s)	κ_a	mobility coefficient of air associated with Darcy's law (dimensionless)
e	void ratio (dimensionless)	κ_l	mobility coefficient of liquid water associated with Darcy's law (dimensionless)
e_0	initial void ratio (dimensionless)	λ'	thermal conductivity of unsaturated medium ($\text{W}/(\text{m } ^{\circ}\text{C})$)
$f(\theta)$	Effective porosity (dimensionless)	λ_{dry}	thermal conductivity of dry soil ($\text{W}/(\text{m } ^{\circ}\text{C})$)
F_v	vapour diffusion enhancement coefficient (dimensionless)	λ_{sat}	thermal conductivity of saturated soil ($\text{W}/(\text{m } ^{\circ}\text{C})$)
G	shear modulus (N/m^2)	μ	Poisson's ratio (dimensionless)
g	gravitational acceleration (m/s^2)	$\xi(\theta)$	temperature gradient ratio (dimensionless)
H	coefficient of solubility of air into water (dimensionless)	ρ_{da}	density of dry air (kg/m^3)
K	bulk modulus (N/m^2)	ρ_l	density of liquid water (kg/m^3)
K_1	hydraulic conductivity (m/s)	ρ_s	density of soil solids (kg/m^3)
L_0	latent heat of evaporation at reference temperature (J/kg)	ρ_v	density of water vapour (kg/m^3)
p_a	air pressure (N/m^2)	σ	total stress (N/m^2)
p_c	capillary pressure (N/m^2)	σ_{ij}	total stress in the ij direction (N/m^2)
p_{cc}	temperature-corrected capillary pressure (N/m^2)	σ_0	reference stress (N/m^2)
p_l	pore water pressure (N/m^2)	τ	tortuosity (dimensionless)
q_{da}	flux of dry air ($\text{kg}/(\text{m}^2 \text{ s})$)	Φ	heat content ($\text{J}/(\text{m}^3 \text{ } ^{\circ}\text{C})$)
q_l	flux of liquid water ($\text{kg}/(\text{m}^2 \text{ s})$)		
q_T	heat flux (W/m^2)		
q_v	flux of water vapour ($\text{kg}/(\text{m}^2 \text{ s})$)		
S_r	degree of saturation (dimensionless)		
S_{ru}	parameter for unsaturated hydraulic conductivity function (dimensionless)		
T	temperature ($^{\circ}\text{C}$)		
T_0	reference temperature ($^{\circ}\text{C}$)		

ABBREVIATIONS

GCL	geosynthetic clay liner
HDPE	high-density polyethylene
MSW	municipal solid waste

REFERENCES

- Abuel-Naga, H. & Bouazza, A. (2010). A novel laboratory technique to determine the water retention curve of geosynthetic clay liners. *Geosynthetics International*, **17**, No. 5, 313–322.
- ASTM D 2435-04. *Standard Test Methods for One-Dimensional Consolidation Properties of Soils Using Incremental Loading*, ASTM International, West Conshohocken, PA, USA.
- Alonso, E. E., Battle, F., Gens, A. & Lloret, A. (1988). Consolidation analysis of partially saturated soils: application to earth dam construction. *Proceedings of the 6th International Conference on Numerical Methods in Geomechanics*, Innsbruck, pp. 1303–1308.

- Beddoe, R. A., Take, W. A. & Rowe, R. K. (2010). Development of suction measurement techniques to quantify the water retention behaviour of GCLs. *Geosynthetics International*, **17**, No. 5, 301–312.
- Beddoe, R. A., Take, W. A. & Rowe, R. K. (2011). Water retention behaviour of geosynthetic clay liners. *Journal of Geotechnical and Geoenvironmental Engineering, ASCE*, [http://dx.doi.org/10.1061/\(ASCE\)GT.1943-5606.0000526](http://dx.doi.org/10.1061/(ASCE)GT.1943-5606.0000526).
- Benson, C. H., Ören, A. H. & Gates, W. P. (2010a). Hydraulic conductivity of two geosynthetic clay liners permeated with a hyperalkaline solution. *Geotextiles and Geomembranes*, **28**, No. 2, 206–218.
- Benson, C. H., Kucukkirca, I. E. & Scalia, J. (2010b). Properties of geosynthetics exhumed from a final cover at a solid waste landfill. *Geotextiles and Geomembranes*, **28**, No. 6, 536–546.
- Barroso, M., Touze-Foltz, N., von Maubeuge, K. & Pierson, P. (2006). Laboratory investigation of flow rate through composite liners consisting of a geomembrane, a GCL and a soil liner. *Geotextiles and Geomembranes*, **24**, No. 3, 139–155.
- Barroso, M., Touze-Foltz, N. & von Maubeuge, K. (2008). Influence of the textured structure of geomembranes on the flow rate through geomembrane-GCL composite liners. *Proceedings of the 4th European Geosynthetics Conference, Eurogeo4*, Edinburgh, 8 pp (CD-ROM).
- Barroso, M. C. P., Lopes, M. G. D. A & Bergamini, G. (2010). Effect of the waste pressure on fluid migration through geomembrane defects. *Proceedings of the 9th International Conference on Geosynthetics*, Guarujá, Brazil, pp. 959–962.
- Bouazza, A. & Vangpaisal, T. (2006). Laboratory investigation of gas leakage rate through a GM/GCL composite liner due to a circular defect in the geomembrane. *Geotextiles and Geomembranes*, **24**, No. 2, 110–115.
- Bouazza, A., Vangpaisal, T., Abuel-Naga, H. & Kodikara, J. (2008). Analytical modelling of gas leakage rate through a geosynthetic clay liner–geomembrane composite liner due to a circular defect in the geomembrane. *Geotextiles and Geomembranes*, **26**, No. 2, 122–129.
- Brachman, R. W. I. & Gudina, S. (2008a). Gravel contacts and geomembrane strains for a GM/CCL composite liner. *Geotextiles and Geomembranes*, **26**, No. 6, 448–459.
- Brachman, R. W. I. & Gudina, S. (2008b). Geomembrane strains from coarse gravel and wrinkles in a GM/GCL composite liner. *Geotextiles and Geomembranes*, **26**, No. 6, 488–497.
- Cartaud, F., Touze-Foltz, N. & Duval, Y. (2005a). Experimental investigation of the influence of a geotextile beneath the geomembrane in a composite liner on the leakage through a hole in the geomembrane. *Geotextiles and Geomembranes*, **23**, No. 2, 117–143.
- Cartaud, F., Goblet, P. & Touze-Foltz, N. (2005b). Numerical simulation of the flow in the interface of a composite bottom liner. *Geotextiles and Geomembranes*, **23**, No. 6, 513–533.
- Cartaud, F., Goblet, P. & Touze-Foltz, N. (2005c). Numerical study of advective flow through composite liners. *Geosynthetics International*, **12**, No. 6, 299–309.
- Delage, P., Sultan, N. & Cui, Y. J. (2000). On the thermal consolidation of Boom clay. *Canadian Geotechnical Journal*, **37**, No. 2, 343–354.
- Devillers, P., Saix, C. & El Youssefi, M. S. (1996). Loi de comportement thermo-hydromécanique pour les sols non saturés: identification in situ des indices de compression thermique. *Canadian Geotechnical Journal*, **33**, No. 2, 250–259.
- de Vries, D. A. (1975). Heat transfer in soils. *Heat and Mass Transfer in the Biosphere, I. Transfer Processes in the Plant Environment*, de Vries, D. A. & Afgan, N., Editors, Scripta Book Company, Washington, DC, pp. 5–28.
- Dickinson, S. & Brachman, R. W. I. (2010). Permeability and internal erosion of a GCL beneath coarse gravel. *Geosynthetics International*, **17**, No. 3, 112–123.
- Döll, P. (1996). *Modelling of moisture movement under the influence of temperature gradients: Desiccation of mineral liners below landfills*, PhD thesis, Technical University of Berlin, Germany.
- Döll, P. (1997). Desiccation of mineral liners below landfills with heat generation. *Journal of Geotechnical and Geoenvironmental Engineering*, **123**, No. 11, 1001–1009.
- El-Zein, A. & Rowe, R. K. (2008). Impact on groundwater of concurrent leakage and diffusion of DCM through geomembranes in landfill liners. *Geosynthetics International*, **15**, No. 1, 55–71.
- Farouki, O. T. (1986). *Thermal Properties of Soils*, Series on Rock and Soil Mechanics, Vol. 11, Trans Tech Publications, Clausthal-Zellerfeld, Germany.
- Fleureau, J.-M., Kheirbek-Saoud, S., Soemitro, R. & Taibi, S. (1993). Behavior of clayey soils on drying–wetting paths. *Canadian Geotechnical Journal*, **30**, No. 2, 287–296.
- Fleureau, J.-M., Verbrugge, J.-C., Huerigo, P. J., Correia, A. G. & Kheirbek-Saoud, S. (2002). Aspects of the behaviour of compacted clayey soils on drying and wetting paths. *Canadian Geotechnical Journal*, **39**, No. 6, 1341–1357.
- Fredlund, D. G. & Rahardjo, H. (1993). *Soil Mechanics for Unsaturated Soils*, Wiley, New York.
- Fredlund, D. G. & Xing, A. (1994). Equations for the soil-water characteristic curve. *Canadian Geotechnical Journal*, **31**, No. 4, 533–546.
- Ghahremannejad, B. (2003). *Thermo-mechanical behaviour of two reconstituted clays*, PhD thesis, University of Sydney, Australia.
- Giroud, J. P. & Touze-Foltz, N. (2003). Geomembranes for landfills. *Geosynthetics International*, **10**, No. 4, 124–133.
- Giroud, J. P. & Touze-Foltz, N. (2005). Equations for calculating the rate of liquid flow through geomembrane defects of uniform width and finite or infinite length. *Geosynthetics International*, **12**, No. 4, 186–199.
- Guyonnet, D., Touze-Foltz, N., Norotte, V., Pothier, C., Didier, G., Gailhanou, H., Blanc, P. & Warmont, F. (2009). Performance-based indicators for controlling geosynthetic clay liners in landfill applications. *Geotextiles and Geomembranes*, **27**, No. 5, 321–331.
- Harpur, W. A., Wilson-Fahmy, R. F. & Koerner, R. M. (1993). Evaluation of the contact between geosynthetic clay liners and geomembranes in terms of transmissivity. *GRI Seminar on Geosynthetic Liner Systems*, IFAI, Philadelphia, PA, pp. 143–154.
- Iryo, T. & Rowe, R. K. (2005). Hydraulic behaviour of soil-geocomposite layers in slopes. *Geosynthetics International*, **12**, No. 3, 145–155.
- Klein, R., Baumann, T., Kahapka, E. & Niessner, R. (2001). Temperature development in a modern municipal solid waste incineration (MSWI) bottom ash landfill with regard to sustainable waste management. *Journal of Hazardous Materials*, **83**, No. 3, 265–280.
- Koerner, J. R. & Koerner, R. M. (1999). *A Survey of Solid Waste Landfill Liner and Cover Regulations. Part II: Worldwide Status*, GRI Report No. 23, Geosynthetics Research Institute, Folsom, PA.
- Koerner, G. R. & Koerner, R. M. (2006). Long-term temperature monitoring of geomembranes at dry and wet landfills. *Geotextiles and Geomembranes*, **24**, No. 1, 72–77.
- Koerner, R. M., Koerner, G. R., Eith, A. W. & Ballod, C. P. (2008). Geomembrane temperature monitoring at dry and wet landfills. *Global Waste Management Symposium*, Colorado (CD-ROM).
- Lake, C. B. & Rowe, R. K. (2000). Swelling of needlepunched, thermally treated GCLs. *Geotextiles and Geomembranes*, **18**, No. 2–4, 77–101.
- Lloret, A. & Alonso, E. E. (1985). State surface for partially saturated soils. *Proceedings of the 11th International Conference on Soil Mechanics and Foundation Engineering*, San Francisco, Vol. 2, pp. 557–562.
- Lange, K., Rowe, R. K. & Jamieson, H. (2010). The potential role of geosynthetic clay liners in mine water treatment systems. *Geotextiles and Geomembranes*, **28**, No. 2, 199–205.
- Mendes, M. J. A., Touze-Foltz, N., Palmeira, E. M. & Pierson, P. (2011a). Influence of structural and material properties of GCLs on interface flow in composite liners due to geomembrane defects. *Geosynthetics International*, **17**, No. 1, 34–47.
- Mendes, M. J. A., Pierson, P., Touze-Foltz, N. & Palmeira, E. M. (2011b). Characterisation of permeability to gas of geosynthetic clay liners in unsaturated conditions. *Geosynthetics International*, **17**, No. 5, 344–354.
- Milly, P. C. D. (1982). Moisture and heat transport in hysteric, inhomogeneous porous media: a heat-based formulation and a numerical model. *Water Resources Research*, **18**, No. 3, 489–498.
- Milly, P. C. D. (1984). A simulation analysis of thermal effects on

- evaporation from soil. *Water Resources Research*, **20**, No. 8, 1087–1098.
- Morris, P. H., Graham, J. & Williams, D. J. (1992). Cracking in drying soils. *Canadian Geotechnical Journal*, **29**, No. 2, 263–277.
- Neiß, J. (1982). *Numerische Simulation des Wärme- und Feuchtetransports und der Eisbildung in Böden*, VDI Verlag, Düsseldorf.
- Paumier, S., Touze-Foltz, N., Pantet, A., Monnet, P., Guyonnet, D., Norotte, V. & Didier, G. (2010). Swell index, oedopermeametric, filter press and rheometric tests to identify the bentonite nature in GCLs. *Geosynthetics International*, **17**, No. 1, 1–11.
- Philip, J. R. & de Vries, D. A. (1957). Moisture movement in porous materials under temperature gradients. *AGU Transactions*, **38**, No. 2, 222–232.
- Rosin-Paumier, S., Touze-Foltz, N. & Pantet, A. (2010a). Impact of a synthetic leachate on permittivity of GCLs measured by filter press and oedopermeameter tests. *Geotextiles and Geomembranes*, **29**, No. 3, 211–221.
- Rosin-Paumier, S., Touze-Foltz, N., Pantet, A., Monnet, P., Didier, G., Guyonnet, D. & Norotte, V. (2010b). Swell index, oedopermeametric, filter press and rheometric tests for identifying the qualification of bentonites used in GCLs. *Geosynthetics International*, **17**, No. 1, 1–11.
- Rowe, R. K. (1998). Geosynthetics and the minimization of contaminant migration through barrier systems beneath solid waste. *Proceedings of the 6th International Conference on Geosynthetics*, Atlanta, GA, March, Industrial Fabrics Association International, St Paul, MN, Vol. 1, pp. 27–103.
- Rowe, R. K. (2005). Long-term performance of contaminant barrier systems: 45th Rankine Lecture. *Géotechnique*, **55**, No. 9, 631–678.
- Rowe, R. K. (2007). Advances and remaining challenges for geosynthetics in geoenvironmental engineering applications: 23rd Manual Rocha Lecture. *Soils and Rocks*, **30**, No. 1, 3–30.
- Rowe, R. K. & Brachman, R. W. I. (2004). Assessment of equivalency of composite liners. *Geosynthetics International*, **11**, No. 4, 273–286.
- Rowe, R. K., Quigley, R. M., Brachman, R. W. I., Booker, J. R. (2004). *Barrier Systems for Waste Disposal Facilities*, Taylor & Francis Books Ltd (E & FN Spon), London, 587 pp.
- Saidi, F., Touze-Foltz, N. & Goblet, P. (2008). Numerical modelling of advective flow through composite liners in case of two interacting adjacent square defects in the geomembrane. *Geotextiles and Geomembranes*, **26**, No. 2, 196–204.
- Saix, C., Devillers, P. & El Yousoufi, M. S. (2000). Éléments de couplage thermomécanique dans la consolidation de sols non saturés. *Canadian Geotechnical Journal*, **37**, No. 2, 308–317.
- Salem, H. S. (2000). Poisson's ratio and the porosity of surface soils and shallow sediments, determined from seismic compressional and shear wave velocities. *Géotechnique*, **50**, No. 4, 461–463.
- Scanlon, B. R. & Milly, P. C. D. (1994). Water and heat fluxes in desert soils. 2: Numerical simulations. *Water Resources Research*, **30**, No. 3, 721–733.
- Southen, J. M. (2005). *Thermally driven moisture movement within and beneath geosynthetic clay liner*, PhD thesis, University of Western Ontario, London, Canada, 320 pp.
- Southen, J. M. & Rowe, R. K. (2005a). Laboratory investigation of GCL desiccation in a composite liner subjected to thermal gradients. *ASCE Journal of Geotechnical and Geoenvironmental Engineering*, **131**, No. 7, 925–935.
- Southen, J. M. & Rowe, R. K. (2005b). Modeling of thermally induced desiccation of geosynthetic clay liners. *Geotextiles and Geomembranes*, **23**, No. 5, 425–442.
- Southen, J. M. & Rowe, R. K. (2007). Evaluation of the soil-water characteristic curve for geosynthetic clay liners. *Geotextiles and Geomembranes*, **25**, No. 1, 2–9.
- Sporer, H. & Gartung, E. (2002). Laboratory tests on desiccation of geosynthetic clay liners. *Proceedings of the International Symposium on Clay Geosynthetic Barriers*, Nuremberg, Germany, pp. 331–338.
- Take, W. A., Chappel, M. J., Brachman, R. W. I. & Rowe, R. K. (2007). Quantifying geomembrane wrinkles using aerial photography and digital image processing. *Geosynthetics International*, **14**, No. 4, 219–227.
- Thomas, H. R. & Missoum, H. (1999). Three-dimensional coupled heat, moisture and air transfer in a deformable unsaturated soil. *International Journal for Numerical Methods in Engineering*, **44**, No. 7, 919–943.
- Thomas, H. R., He, Y., Sansom, M. R. & Li, C. L. W. (1996). On the development of a model of the thermo-mechanical-hydraulic behavior of unsaturated soils. *Engineering Geology*, **41**, No. 14, 197–218.
- Thusyanthan, N. I., Madabhushi, S. P. G. & Singh, S. (2007). Tension in geomembranes on landfill slopes under static and earthquake loading-centrifuge study. *Geotextiles and Geomembranes*, **25**, No. 2, 78–95.
- Touze-Foltz, N. (2002). The influence of non-uniform transmissivity vis-à-vis hole location. *Geotextiles and Geomembranes*, **20**, No. 4, 263–277.
- Touze-Foltz, N. & Barroso, M. (2006). Empirical equations for calculating the rate of liquid flow through geosynthetic clay liners–geomembrane composite liners. *Geosynthetics International*, **13**, No. 2, 73–82.
- Touze-Foltz, N. & Giroud, J. P. (2003). Empirical equations for calculating the rate of liquid flow through composite liners due to geomembrane defects. *Geosynthetics International*, **10**, No. 6, 215–233.
- Touze-Foltz, N. & Giroud, J. P. (2005). Empirical equations for calculating the rate of liquid flow through composite liners due to large circular defects in the geomembrane. *Geosynthetics International*, **12**, No. 4, 205–207.
- Touze-Foltz, N., Rowe, R. K. & Navarro, N. (2001). Liquid flow through composite liners due to geomembrane defects: Nonuniform hydraulic transmissivity at the liner interface. *Geosynthetics International*, **8**, No. 1, 1–26.
- Touze-Foltz, N., Duquennoi, C. & Gaget, E. (2006). Hydraulic and mechanical behavior of GCLs in contact with leachate as part of a composite liner. *Geotextiles and Geomembranes*, **24**, No. 3, 188–197.
- van Genuchten, M. Th. (1980). A closed-form equation for predicting the hydraulic conductivity of unsaturated soils. *Soil Science Society of America Journal*, **44**, No. 5, 892–898.
- Yoshida, H. & Rowe, R. K. (2003). Consideration of landfill liner temperature. *Proceedings of the 8th International Waste Management and Landfill Symposium*, S. Margherita di Pula, Cagliari, Sardinia, Italy, October, CD-ROM, 9 pp.
- Zhou, Y. & Rowe, R. K. (2003). Development of a technique for modelling clay liner desiccation. *International Journal for Numerical and Analytical Methods in Geomechanics*, **27**, No. 6, 473–493.
- Zhou, Y. & Rowe, R. K. (2005). Modelling of clay liner desiccation. *ASCE Journal of Geomechanics*, **5**, No. 1, 1–9.

The Editor welcomes discussion on all papers published in *Geosynthetics International*. Please email your contribution to discussion@geosynthetics-international.com by 15 April 2012.